Table 6. *Summary of bond and lone-pair peak heights* (e Å^{-3}) *in experimental and theoretical electron density maps*

	Experimental			Theoretical	
Dynamic density	$X+N$ model	X model	$X-N$	4-31G	EBS
C(1)–C(1′)	0·57	0·57	0·69	0·38	0·58
C(1)–O(1)	0·47	0·48	0·49	0·20	0·43
C(1)–O(2)	0·59	0·62	0·55	0·46	0·62
O(1)–H(1)	0·35	0·33	0·33	0·23	0·40
O(1) l.p.	0·45	0·37	0·49	0·73	0·60
O(2) l.p.	0·35	0·28	0·41	0·61	0·53
O(2) l.p.	0·29	0·25	0·31	0·64	0·53
Static density					
C(1)–C(1′)	0·64	0·65		0·40	0·67
C(1)–O(1)	0·58	0·60		0·25	0·54
C(1)–O(2)	0·79	0·85		0·54	0·70
O(1)–H(1)	0·62	0·55		0·34	0·56
O(1) l.p.	0·93	0·68		1·18	1·10
O(2) l.p.	0·61	0·44		1·49	1·22
O(2) l.p.	0·54	0·42		1·39	1·32

The authors would like to thank Drs Koetzle and McMullen from Brookhaven National Laboratory for making the neutron data on oxalic acid dihydrate available. Support of this work by the National Science Foundation (CHE7905897) is gratefully acknowledged.

References

BATS, J. W., COPPENS, P. & KOETZLE, T. F. (1977). *Acta Cryst.* B**33**, 37–45.
BATS, J. W., COPPENS, P. & KVICK, A. (1977). *Acta Cryst.* B**33**, 1534–1542.
COPPENS, P. (1968). *Acta Cryst.* B**24**, 1272–1274.
COPPENS, P. (1974). *Acta Cryst.* B**30**, 255–261.
COPPENS, P., MOSS, G. & HANSEN, N. K. (1980). In *Computing in Crystallography*, edited by R. DIAMOND, S. RAMASESHAN & K. VENKATESAN. Bangalore: Indian Academy of Sciences.
CRAVEN, B. M. & MCMULLAN, R. K. (1979). *Acta Cryst.* B**25**, 934–945.
HANSEN, N. K. & COPPENS, P. (1978). *Acta Cryst.* A**34**, 909.
HIRSHFELD, F. L. (1977). *Isr. J. Chem.* **16**, 226–231.
MCCANDLISH, L. E., STOUT, G. H. & ANDREWS, L. C. (1975). *Acta Cryst.* A**31**, 245–249.
MCMULLEN, R. K. & KOETZLE, T. F. (1980). Unpublished results.
MULLEN, D. (1980). *Acta Cryst.* B**36**, 1610–1615.
REES, B. (1976). *Acta Cryst.* A**32**, 483–488.
SAVARIAULT, J. M. & LEHMANN, M. S. (1980). *J. Am. Chem. Soc.* **102**, 1298–1307.
STEVENS, E. D. (1980). *Acta Cryst.* B**36**, 1876–1887.
STEVENS, E. D. & COPPENS, P. (1980). *Acta Cryst.* B**36**, 1864–1876.
STEWART, R. F. (1976). *Acta Cryst.* A**32**, 565–574.
THOMAS, J. O. (1978). *Acta Cryst.* A**34**, 819–823.

Acta Cryst. (1981). A**37**, 863–871

Direct Observation of TDS Profiles from Perfect Silicon Single Crystals on a Neutron Diffractometer

BY HANS A. GRAF AND JOCHEN R. SCHNEIDER

Hahn-Meitner-Institut für Kernforschung, Glienicker Strasse 100, *D*-1000 *Berlin* 39, *Federal Republic of Germany*

AND ANDREAS K. FREUND AND MOGENS S. LEHMANN

Institut Max von Laue–Paul Langevin, 156*X*, *F*-38042 *Grenoble CEDEX, France*

(*Received* 9 *January* 1981; *accepted* 5 *May* 1981)

Abstract

TDS profiles convoluted with the instrument resolution were obtained by forming differences between diffraction profiles measured with neutrons of wavelength 0·60 Å on three perfect Si crystals of different thickness. The profiles were measured with two detector apertures for the reflections 022, 004, 044, 026, 008 and 066. From these measurements TDS correction factors α and hence a correction term ΔB for the temperature parameter of Si were derived. The temperature parameter of Si was determined for two temperatures, 92 and 292 K, as $B_{92} = 0{\cdot}212\ (3)$ Å^2 and $B_{292} = 0{\cdot}422\ (3)$ Å^2, respectively, from the refinement of 100 symmetry-inequivalent reflections measured with neutrons of wavelength 0·53 Å on an imperfect Si crystal.

0567-7394/81/060863-09$01.00

1. Introduction

This work is part of systematic investigations exploring the possibilities offered by the hot-source four-circle neutron diffractometer D9 at the Institut Laue–Langevin (ILL). With neutrons of wavelength $\lambda = 0{\cdot}5$ Å or lower, available at this instrument, reflections of $\sin\theta/\lambda$ values beyond 2 Å^{-1} can be measured. In principle, one should obtain very accurate temperature parameters from such high-resolution data. In order to check this experimentally we have studied silicon. For this material very accurate temperature parameters at room temperature and at 92 K are known from X-ray *Pendellösung* measurements (Aldred & Hart, 1973). The temperature parameters, however, which we have determined with short-wavelength neutrons on a nearly ideally imperfect silicon crystal were systematically lower than the *Pendellösung* values. We believe that this disagreement is an effect of thermal diffuse scattering (TDS).

Following the experiments on the imperfect crystal, we have therefore attempted to measure directly the TDS in silicon with perfect single-crystal plates. From these measurements the relative amount of TDS, α_{TDS}, at room temperature can be estimated for the kinematical case, and the usual approximation can be used to correct the temperature parameters obtained from our measurements on the imperfect silicon crystal.

2. Experiments on the imperfect silicon crystal

The imperfect silicon crystal used for the measurements had dimensions 3 × 3 × 3 mm and was cut from a large silicon crystal which had been plastically deformed at 1253 K in a hot pressing device. The experiments were carried out at the D9 four-circle diffractometer of the ILL with a neutron wavelength of 0·53 Å both at room temperature (292 K) and at low temperature (92 K). The reflections were recorded in coupled θ–2θ step scans where the total scan range varied from 1·2° at low angles to 4·8° at 100° in 2θ. For both temperatures, reflections with $h, k, l \geq 0$ were measured for values of $\sin\theta/\lambda \leq 1{\cdot}45$ Å^{-1}, and, after averaging, a total of 100 symmetry-independent reflections were left. Absorption corrections were not necessary and also multiple scattering processes could be neglected as no evidence of such events was detected at measurements of forbidden reflections with $h + k + l = 4n + 2$.

The refinement procedure used the least-squares program *LINEX* (Coppens, 1974) minimizing the quantity $\sum w(F_o^2 - k^2F_c^2)^2$, where $w = 1/[\sigma^2(\text{counting}) + (0{\cdot}015F_o^2)]$, k is the scale factor, and F_o and F_c are the observed and calculated structure factors, respectively. A scattering length of $0{\cdot}4149 \times 10^{-14}$ m (Shull & Oberteuffer, 1972) was used for F_c, and the extinction correction was assumed to be isotropic with a Gaussian mosaic distribution. Extinction effects were very small; the largest reduction of only 7% in intensity was observed at the 022 reflection. Final parameters (B_n) and agreement factors are given in Table 1 together with the X-ray results (B_x) of Aldred & Hart (1973). Our B values are significantly lower than the corresponding X-ray values and the difference $B_x - B_n$ increases with temperature, as one would expect when TDS is the source of these discrepancies.

3. Measurements on perfect silicon crystals

3.1. *The method of obtaining TDS profiles*

If the thickness of perfect single-crystal plates studied in a diffraction experiment is much larger than the so-called extinction length (Zachariasen, 1945), the integrated reflecting power for elastic scattering, R_{dyn}, becomes, in a first approximation, independent of crystal thickness. The weak thermal diffuse scattering, however, is adequately described by the kinematical scattering theory (Nilsson, 1957) and thus depends on the crystal volume irradiated by the neutron or X-ray beam. Therefore, the TDS intensity, R_{TDS}, is proportional to the crystal thickness. By measuring the same Bragg reflections on perfect single crystals of different thickness and subtracting the recorded profiles, the contribution from elastic scattering cancels and one obtains TDS profiles, convoluted with the instrument resolution.

We have chosen the symmetric Laue geometry for our experiments on perfect single-crystal plates in order to keep the geometrical beam widening small at low Bragg angles and to have the simple expression $\exp(-\mu_t t_0/\cos\theta)$ for the absorption correction, where t_0 is the crystal thickness and μ_t represents the linear coefficient of total attenuation including nuclear capture and incoherent and inelastic scattering processes in the case of neutrons. The coefficient μ_t is small for silicon but not negligible and was determined experimentally. On the other hand, the integrated reflecting power, R_{dyn}, in Laue geometry may not be regarded as virtually independent of crystal thickness with respect to the crystals used in our experiments, as would be the

Table 1. *Temperature parameters B_n and agreement factors from the refinement of* 100 *symmetry-inequivalent reflections measured on a nearly ideally imperfect* Si *crystal*

The Debye–Waller factor is defined as $\exp[-B(\sin\theta/\lambda)^2]$, the R factor as $\sum|F_o - F_c|/\sum F_o$ and the goodness-of-fit G as $[\sum w|F_o^2 - F_c^2|/(n-m)]^{1/2}$. B_x are the temperature parameters given by Aldred & Hart (1973).

Temperature (K)	R	G	B_n	B_x	$B_x - B_n$
92	0·009	0·99	0·212 (3)	0·227 (3)	0·015
292	0·011	0·94	0·422 (3)	0·461 (3)	0·039

case when measuring in Bragg geometry. This aspect together with the instrument resolution is discussed in more detail in the Appendix.

3.2. *Measurement of the reflection profiles*

Three perfect Si crystal discs *A*, *B* and *C* manufactured by Wacker Chemie, Burghausen, of diameter 80 mm and thicknesses of 3·74, 6·94 and 10·05 mm, respectively, were used for the measurements. These discs had been cut parallel to the (001) lattice planes and the surfaces had been chemically polished in order to remove damage introduced by sawing. Their perfection was confirmed by X-ray topography and X-ray rocking-curve measurements. The neutron scattering experiments were then performed at the four-circle diffractometer D9 of the Institut Laue–Langevin under experimental conditions which were kept as close as possible to those of the measurements on the imperfect silicon crystal described above.

The perfect silicon crystals were studied in symmetric Laue geometry at room temperature with a wavelength of 0·60 Å. A circular aperture of 4 mm diameter limited the beam immediately before the sample and a circular aperture of 12 mm diameter defined the scattered beam in front of the detector. The distance from detector to sample was 175 mm for one series of measurements (large aperture) and 350 mm for another series of measurements (small aperture), corresponding to solid angles at the sample of $3{\cdot}69 \times 10^{-3}$ and $9{\cdot}23 \times 10^{-4}$ rad^2, respectively. The crystals were mounted with their [001] axis near, but not parallel to, the φ axis of the diffractometer. Three symmetry-equivalent reflections belonging to the lattice planes (022), (004), (044), (026), (008) and (066) were recorded on each crystal in coupled θ–2θ scans for a constant number of monitor counts. The scans consisted of background measurements with 17 points on both sides of the elastic peak at constant stepwidth of 0·2° and a central part with 27 points and a stepwidth increasing with the Bragg angle according to the resolution function of the instrument. The angular range of the central part varied from 1·3° at low Bragg angles to 2·9° at high Bragg angles. For the small-aperture measurements the central part of each reflection was recorded a second time with a finer scan grid of 41 points.

Although nuclear absorption ($\mu_{abs} = 0{\cdot}02$ mm^{-1} at $\lambda = 0{\cdot}6$ Å) is very small, a correction must be made for the total attenuation mainly coming from inelastic scattering processes. Therefore, we determined experimentally the corresponding linear attenuation coefficient μ_t from transmission measurements on the three crystals with 0·53 Å neutrons at room temperature. μ_t was obtained as 0·76 (1) mm^{-1} in agreement with other measurements (Brugger, 1976; Freund, 1980). The slight variation of μ_t from $\lambda = 0{\cdot}53$ to $\lambda = 0{\cdot}60$ Å can be neglected. We assume that the attenuation due to inelastic scattering processes affects the dynamical diffraction phenomena in the crystal only to a negligible amount.

3.3. *The averaged reflection profiles*

An absorption correction was applied to the data according to the expression $\exp(-\mu_t t_0/\cos\theta)$. The profiles were corrected for setting errors by determining the peak position from the mean ω angle of the peak width at half maximum. All intensities recorded for symmetry-equivalent reflections on the same crystal and with the same detector aperture were then combined into one profile to which a spline function was fitted. The least-squares spline-function algorithm used in this procedure permitted the construction of averaged reflection profiles with the same mesh as the originally measured scans. The combined errors arising from both statistics and from the fitting procedure were estimated by determining the deviations of the measured intensities from the spline function and dividing them up amongst the points of the averaged reflection profile. A standard deviation was then evaluated for each point of the averaged profile according to sample statistics.

In Figs. 1 and 2 we show superimposed three 022 and three 066 rocking curves measured with the large and the small detector aperture, respectively. The curves *a*, *b* and *c* on each figure correspond to the three crystals *A*, *B* and *C* of different thicknesses. The amount of TDS which is due to the difference in crystal thickness is represented by the area between the rocking curves *a*, *b* and *c*, assuming that the elastic scattering is the same for all three crystals. By comparing the two reflections 022 and 066 which define the lower and upper limits, respectively, of the $\sin\theta/\lambda$ range in our measurements on the perfect silicon crystals, it can be seen that TDS is much more

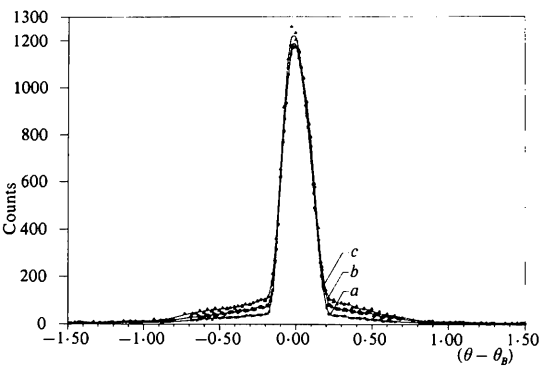

Fig. 1. 022 rocking curves *a*, *b* and *c* (θ–2θ scan) measured with the large detector aperture on the three crystals *A*, *B* and *C*, respectively. The symbols denote the experimental points from several scans (counts/100 000 monitor counts). The full lines are the spline functions fitted to the data.

important at higher scattering angles. However, the TDS contribution to the reflection 022 is still clearly visible in the far-ranging tails on both sides of the elastic peak. The shape of the elastic peak in Figs. 1 and 2 reflects the resolution function of the instrument at the particular Bragg angle.

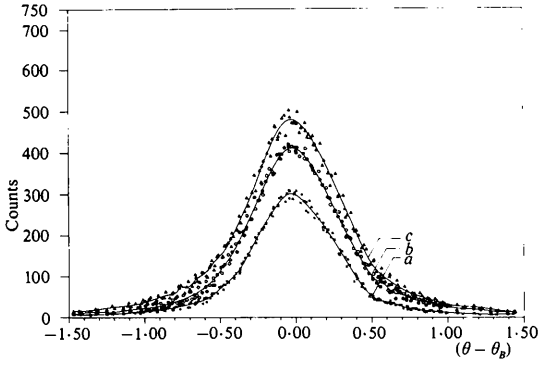

Fig. 2. 066 rocking curves *a*, *b* and *c* (θ–2θ scan) measured with the small detector aperture on the three crystals *A*, *B* and *C*, respectively. The symbols denote the experimental points from several scans (counts/100 000 monitor counts). The full lines are the spline functions fitted to the data.

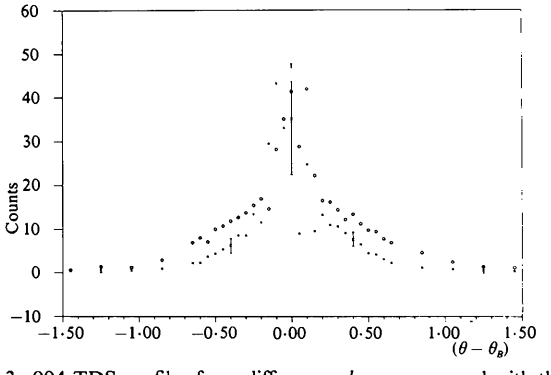

Fig. 3. 004 TDS profiles from differences $b - a$ measured with the small (crosses) and the large (circles) detector aperture. The intensities (counts/100 000 monitor counts) are normalized to a difference crystal thickness of 1 mm. The error bars show $\pm S_s$.

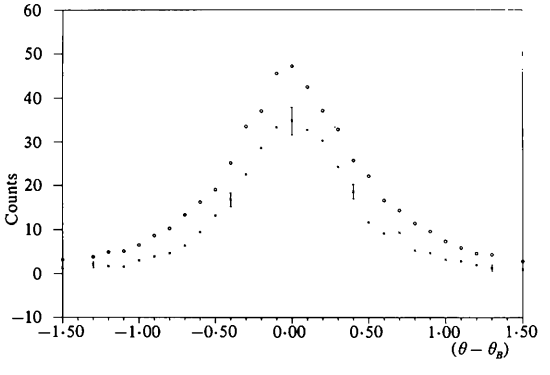

Fig. 4. 008 TDS profiles from differences $b - a$ measured with the small (crosses) and the large (circles) detector aperture. The intensities (counts/100 000 monitor counts) are normalized to a difference crystal thickness of 1 mm. The error bars show $\pm S_s$.

3.4. *The TDS profiles*

By forming differences between the averaged reflection profiles *a*, *b* and *c* we obtained for each reflection and for both detector apertures the two difference profiles $b - a$ and $c - b$. These profiles were normalized to the same scattering volume by multiplying the differences with $\cos\theta/\Delta t_0$. They represent experimental TDS profiles convoluted with instrument resolution. Examples of such difference profiles are shown in Figs. 3, 4 and 5. Fig. 3 represents the 004 profiles $b - a$ measured with both detector apertures. The errors are large in the region of the very narrow elastic peak where the averaging procedure is sensitive to small angular shifts in the original profiles, and where we are calculating small differences of large numbers. The 004 reflection is close to the minimum in the instrument resolution. As the elastic peak broadens owing to dispersion effects and the relative TDS contribution increases with increasing Bragg angle, the difference profiles of the higher-order reflections, *i.e.* 008 and 066 become much smoother, like the curves given in Fig. 4. These curves represent the $b - a$ profiles corresponding to the 008 reflection measured with both detector apertures.

A dip occurs at the center of the $b - a$ difference profile of the reflection 022 shown in Fig. 5. It appears also in the other difference profiles of the same reflection. O'Connor & Butt (1963) and Zasimov, Lobanov, Rüdiger & Kusmin (1976) have observed similar behaviour in TDS profiles recorded by the Mössbauer technique. Bärnighausen (1978) ascribes this feature to experimental difficulties in the Mössbauer technique. In our case the dip is not significant when taking into account the large errors at the position of the elastic peak shown in Fig. 5, and we cannot assign to it any physical meaning.

3.5. *TDS intensities and experimental values for* α

The difference profiles were integrated after the usual background corrections in order to obtain the one-phonon TDS intensities. The integration range (see Table 4) was chosen to include the whole peak up to points where the tails were running into a flat, uniform

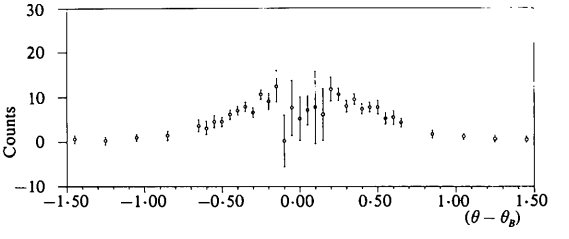

Fig. 5. 022 TDS profile from the difference $b - a$ measured with the large detector aperture. The intensities (counts/100 000 monitor counts) are normalized to a difference crystal thickness of 1 mm. The error bars show $\pm S_s$.

background. The limits were set by visual inspection of the profiles. The background, which includes multiphonon and incoherent scattering, was approximated by a straight line fitted to the data outside the peak and then subtracted from the total intensity. The TDS correction factor α is defined by

$$I_{meas} = I_{Bragg}(1 + \alpha) = I_{Bragg} + I_{TDS}. \quad (1)$$

Equation (1) can be expressed as $\alpha = I_{TDS}/(I_{meas} - I_{TDS})$. In order to evaluate α one has to know I_{meas} for the same experimental conditions under which I_{TDS} has been obtained. We have determined values of I_{meas} with the large detector aperture on a large imperfect-crystal plate of 2 mm thickness produced in the same way as the 3 × 3 × 3 mm crystal. The intensities I_{meas} are listed in Table 2 together with the TDS intensities, I_{TDS}, all normalized to the same scattering volume.

The experimental TDS correction factors α are listed in Table 3. The error made by combining TDS intensities measured with the small detector aperture with values of I_{meas} determined with the large detector aperture can be neglected. The large standard deviations, S_s, for the values of α listed in Table 3 come from the errors in I_{TDS} which are basically due to the evaluation of small differences from large numbers. A second set of errors denoted as S_{osc} is listed in Table 3. These errors represent the maximum uncertainties introduced by oscillations of the dynamic reflecting power R_{dyn} as discussed in the Appendix. The estimate of the total error in the experimental values for α obtained by adding S_s and S_{osc} seems to be rather pessimistic.

Table 2. *Experimental TDS intensities I_{TDS} and intensities I_{meas} measured on a large imperfect* Si *crystal plate*

All intensities are normalized to the same scattering volume corresponding to a crystal thickness of 1 mm. In brackets standard deviations derived from sample statistics (I_{TDS}) or counting statistics (I_{meas}), respectively, are given.

		I_{TDS}				I_{meas}
		Small aperture		Large aperture		
h k l	θ_B	*b* − *a*	*c* − *b*	*b* − *a*	*c* − *b*	
0 2 2	8·99	7 (18)	9 (48)	10 (12)	23 (16)	5079 (102)
0 0 4	12·77	17 (22)	13 (27)	26 (13)	23 (13)	3714 (74)
0 4 4	18·21	23 (8)	18 (10)	36 (13)	30 (21)	2173 (44)
0 2 6	20·45	24 (5)	23 (8)	39 (8)	40 (13)	1972 (40)
0 0 8	26·23	34 (6)	28 (10)	54 (11)	41 (15)	1302 (26)
0 6 6	27·95	33 (5)	24 (8)	48 (11)	43 (13)	1156 (23)

4. Discussion of the experimental results and comparison with calculation

4.1. *Theoretical background*

The primary objective of our experiments was to determine an overall correction term ΔB for the temperature factor B in silicon from measured TDS intensities.

In the simplest approximation (see Willis, 1969) the TDS correction factor α is only a fraction of $(\sin\theta/\lambda)^2$:

$$\alpha = C(\sin\theta/\lambda)^2. \quad (2)$$

In this derivation the elastic waves in the crystal are assumed to propagate isotropically, and the volume in reciprocal space covered during a scan is taken to be a sphere of radius q_{max}. The coefficient C is proportional to the temperature and to q_{max}.

For small α values $(1 + \alpha)$ in (1) can be replaced by $\exp\alpha$. The correction for the TDS contamination of the Bragg intensities thus reduces to a correction ΔB applied to the temperature factor (Willis, 1969):

$$|F_{obs}|^2 = |F|^2 \exp[-2(B - \Delta B)\sin^2\theta/\lambda^2] \quad (3)$$

with $\Delta B = C/2$ from (2). Accordingly, the temperature factor found in a conventional refinement is too small by ΔB if no TDS correction has been applied to the measured intensities. This method of deriving an overall correction term ΔB implies approximations which are in general very unrealistic in an actual neutron experiment, the main difficulty arising from the fact that the volume τ^* covered in reciprocal space during a scan is not fixed. It is angle dependent and, in addition, the scan range is usually changed in a series of measurements according to the resolution function of

Table 3. *Experimental α values derived from the difference $b - a$ (α_{b-a}) and $c - b$ (α_{c-b}) for both detector apertures*

S_s is the standard deviation derived from sample statistics and S_{osc} is the maximum error introduced by the oscillations of the dynamic reflecting power R'_H. S_s and S_{osc} are given in units of the last digit of the α values.

	Small aperture						Large aperture					
h k l	α_{b-a}	S_s	S_{osc}	α_{c-b}	S_s	S_{osc}	α_{b-a}	S_s	S_{osc}	α_{c-b}	S_s	S_{osc}
0 2 2	0·001	3	1	0·002	9	0	0·002	2	1	0·005	3	0
0 0 4	0·005	6	1	0·004	7	0	0·007	3	1	0·006	4	0
0 4 4	0·011	4	2	0·008	5	1	0·017	6	2	0·014	10	1
0 2 6	0·012	2	2	0·012	4	1	0·020	4	2	0·021	7	1
0 0 8	0·027	5	3	0·022	4	2	0·043	9	4	0·033	13	3
0 6 6	0·029	5	4	0·021	7	3	0·043	13	5	0·039	13	3

the instrument. In a θ–2θ scan, as used in our experiment, τ^* is well approximated by a parallelepiped given by

$$\tau^* = (2\pi/\lambda)^3 \beta_h \beta_v \Delta\omega \sin 2\theta \qquad (4)$$

assuming a rectangular receiving slit in front of the detector with horizontal aperture β_h and vertical aperture β_v; $\Delta\omega$ is the total scan range.

In the X-ray case where the scattering surface for one-phonon processes is nearly identical to the Ewald sphere, all phonon wave numbers **q** inside τ^* contribute to the TDS intensity. In the neutron case, however, the one-phonon scattering surfaces are hyperboloids for faster-than-sound neutrons ($\beta < 1$) and ellipsoids for slower-than-sound neutrons ($\beta > 1$), where β is the ratio of the phonon velocity to the neutron velocity (Seeger & Teller, 1942; Willis, 1970; Cooper, 1971). The case $\beta < 1$ can be approximately treated like the X-ray case (Willis, 1970) and integration over τ^* should be satisfactory. For slower-than-sound neutrons, the TDS intensity is constant during the scan over an angular region $\delta\theta$, over which the whole ellipsoid representing the scattering surface is seen by the detector (Cooper, 1971). If $\delta\theta$ is small compared to the total scan range $\Delta\omega$, then this case can again approximately be treated like the X-ray case (Larsen, Lehmann & Merisalo, 1980).

The wavelengths used in our measurements on the imperfect crystal and on the perfect crystal plates correspond to neutron velocities of 7460 and 6600 m s^{-1}, respectively. From the elastic constants of Si (McSkimin, 1953) the velocity of longitudinal and transverse phonons in the [100] direction can be estimated to be ~8400 and ~5840 m s^{-1}, respectively. The neutron velocity in both measurements is thus between the phonon velocities and the case $\beta > 1$ must be considered for some of the phonons. The constant TDS intensity range $\delta\theta$ for $\beta > 1$ phonons can be estimated (Cooper, 1971) to be $\pm 0{\cdot}4$ and $\pm 0{\cdot}8°$ for the measurements with the small and the large aperture, respectively, and is thus smaller than the scan range of $\pm 1{\cdot}75$ to $\pm 2{\cdot}5°$ over which the TDS intensity has been integrated. Within an elastically isotropic approximation, a TDS calculation as in the X-ray case, including all phonons and allowing for the actual scan volumes, τ^*_{hkl}, should therefore give the closest agreement with the experimental results.

4.2. *Derivation of ΔB*

According to (2) the correction term ΔB can be found by plotting α against $(\sin\theta/\lambda)^2$. The slope of a straight line through the origin fitted to the experimental points should then give a mean value for $2\Delta B$. A spherical scan volume of the same radius q_{max} for all reflections hkl, however, has been assumed in deriving (2). It is a more realistic approach to fit a sphere to the actual scan volume τ^*_{hkl} given by (4) and derive an individual radius $q_{max}(hkl) = (3\tau^*_{hkl}/4\pi)^{1/3}$ for each reflection [values of $q_{max}(hkl)$ applying to our experimental conditions are listed in Table 4]. A good fit to a straight line is now obtained when the experimental α values are normalized to a common q_{max} value. This is shown in Fig. 6 where the α_{b-a} values for both detector apertures have been scaled by $q_{max}(066)/q_{max}(hkl)$. The α_{b-a} values were preferred for this fit because we believe that the α_{c-b} values, which are derived from the thicker crystals, are possibly affected by multiple scattering at high $(\sin\theta/\lambda)^2$ and $q_{max}(066)$ was used for scaling, as the reciprocal volume covered during a scan through the reflection 066 with the small detector aperture is comparable to the reciprocal volume involved in measuring the higher-order reflections on the imperfect silicon cube.

Assuming that the temperature-factor refinement is mainly affected by these high-order reflections, we can estimate an effective q_{max} value of $q_{eff} \simeq 0{\cdot}32$ Å^{-1} for the data set collected on the imperfect silicon crystal ($\beta_h = \beta_v = 3{\cdot}31 \times 10^{-2}$ rad, scan range $\Delta\omega = 4{\cdot}8°$, $2\theta_{mean} = 120°$, $\lambda = 0{\cdot}53$ Å). From Fig. 6 we find a slope $2\Delta B' = 0{\cdot}046$ (13) Å^2 of the straight line fitted to the small aperture α_{b-a} values which had been normalized to $q_{max}(066) = 0{\cdot}264$ Å^{-1}. The error has

Table 4. *Calculated α values*

$\Delta\omega$ is the angular range over which the TDS profiles have been integrated and $q_{max}(hkl)$ is the q_{max} value within the spherical isotropic approximation calculated for the actual scan volume τ^*_{hkl}. α_q has been calculated within the spherical isotropic approximation with $q_{max}(hkl)$; $\alpha_{X\text{-ray}}$ and $\alpha_{\beta<1}$ have been calculated with the program of Merisalo & Kurittu (1978) including all phonons ($\alpha_{X\text{-ray}}$) or only $\beta < 1$ phonons ($\alpha_{\beta<1}$), respectively.

	Integration range	Small aperture				Large aperture			
$h\ k\ l$	$\Delta\omega$ (°) (both apertures)	$q_{max}(hkl)$ (Å^{-1})	α_q	$\alpha_{X\text{-ray}}$	$\alpha_{\beta<1}$	$q_{max}(hkl)$ (Å^{-1})	α_q	$\alpha_{X\text{-ray}}$	$\alpha_{\beta<1}$
0 2 2	±1·75	0·168	0·003	0·0021	0·0018	0·267	0·004	0·0036	0·0030
0 0 4	±2·00	0·197	0·006	0·0049	0·0039	0·312	0·009	0·0092	0·0076
0 4 4	±2·25	0·228	0·014	0·0121	0·0093	0·362	0·022	0·0231	0·0189
0 2 6	±2·25	0·235	0·018	0·0167	0·0130	0·374	0·028	0·0310	0·0256
0 0 8	±2·50	0·260	0·031	0·0311	0·0247	0·412	0·050	0·0577	0·0480
0 6 6	±2·50	0·264	0·036	0·0352	0·0275	0·418	0·057	0·0659	0·0544

been estimated rather pessimistically from the error bars as indicated in Fig. 6. With the scale factor $q_{\text{eff}}/q_{\max}(066)$, the correction ΔB is calculated to be 0·028 (8) Å^2. The temperature factor $B = 0{\cdot}422$ (3) Å^2 determined from a conventional refinement of Bragg intensities not corrected for TDS is thus increased to $B_{\text{corr}} = 0{\cdot}450$ (11) Å^2. This value is now in reasonable agreement with the very precise value $B = 0{\cdot}461$ (3) Å^2 determined by Aldred & Hart (1973) from *Pendellösung* measurements. Within the approximation of (2) ΔB is directly proportional to the absolute temperature. The correction for the low-temperature measurement (92 K) can thus be determined by linear extrapolation as $\Delta B_{92} = 0{\cdot}009$ (3) Å^2. The corrected low-temperature B value is then 0·221 (6) Å^2 which agrees with the value of Aldred & Hart of $B_x = 0{\cdot}227$ (3) Å^2 within the experimental error.

4.3. *Calculated values of* α

We have calculated two sets of TDS correction factors, $\alpha_{\text{X-ray}}$ and $\alpha_{\beta<1}$, with a computer program for anisotropic one-phonon TDS correction (Merisalo & Kurittu, 1978). The program takes into account the volume in reciprocal space covered during a symmetric ω scan or θ–2θ scan and allowance can be made for the background correction. The results are strictly valid for the X-ray case within the long-wavelength, continuum elasticity approximation. The $\alpha_{\text{X-ray}}$ values include contributions from all phonons, the $\alpha_{\beta<1}$ values include only contributions from phonons with velocities slower than the neutron velocity. The $\alpha_{\beta<1}$ values represent the lower limits expected for a TDS correction in the neutron case. In the calculations, the circular apertures used in our measurements were approximated by square apertures of the same area. The α values calculated in this manner for both detector apertures are listed in Table 4. For comparison we have included in Table 4 also α_q values, which were calculated within the spherical isotropic approximation (Willis, 1969) using the $q_{\max}(hkl)$ values applying to the actual scan volumes instead of a fixed $q_{\max}$ value. A background subtraction was assumed in all these calculations and the elastic constants for silicon were taken from McSkimin (1953).

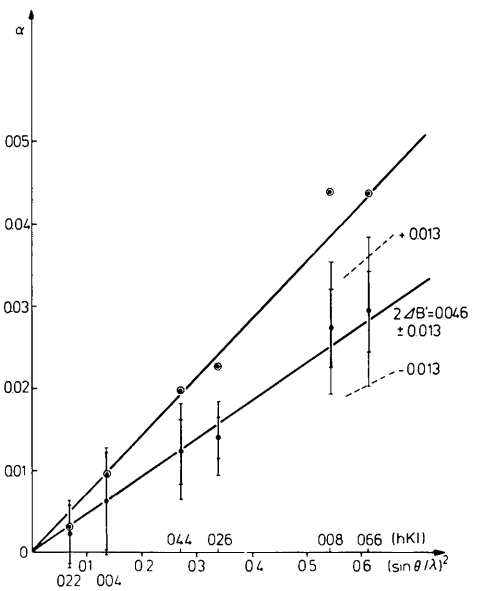

Fig. 6. Experimental α_{b-a} values from the small-aperture (full circles) and the large-aperture measurements (open circles with dots) scaled to the reciprocal volume τ^*_{066} (small aperture) and τ^*_{066} (large aperture), respectively. The straight lines were fitted to these scaled α_{b-a} values. From the slope of the lower line the correction term $2\Delta B'$ has been obtained. The error bars show $\pm S_s$ (inner part) and $\pm S_{\text{osc}}$ (outer part). The scale factor between the slopes of the two lines is found to be 1·54, in good agreement with the calculated value of 1·58 which is given by the ratio of the $q_{\max}(066)$ values for the two detector apertures.

The limited accuracy of our experimental results does not allow us to discriminate strictly between the three sets of calculated values. They all fit the observed data within the errors. There are only minor differences between the α_q and $\alpha_{\text{X-ray}}$ values, but these calculated values are larger than those observed. Rather good agreement is obtained between observed α and $\alpha_{\beta<1}$ values. This possibly indicates that including contributions from phonons with velocities faster than the neutron velocity leads to an overestimation of the TDS correction, in contrast to the arguments given at the end of § 4.1. At high $(\sin\theta/\lambda)^2$, however, the $\alpha_{\beta<1}$ values are still larger than the α_{c-b} values. We believe that the main reason for these systematic deviations is multiple scattering, which tends to reduce the inelastic, kinematical scattering from a thick crystal more than from a thin crystal. It is, however, possible that the discrepancies are also partly due to small truncation effects coming from the large spot size at high Bragg angles. The spot size in the horizontal plane is the crystal size seen by the detector for a narrow beam, $t_0 \tan\theta$, convoluted with the beam broadening. The size of the detector entrance window chosen for the measurements was comparable to the spot size of the reflection 066, and as long as the reflection spot is in the middle of the detector no loss would occur. It is, however, likely that the true coupling between crystal rotation θ and spot location on the detector is less than two as assumed in the θ–2θ scan. This would lead to a loss of the tails of the TDS profile.

5. Conclusions

We have demonstrated a method of obtaining TDS profiles from neutron scattering on perfect crystals with a classical four-circle diffractometer. The measurements allowed us to derive experimental TDS correction factors α and, hence, a correction term ΔB for the

Table 5. *Relative momentum spread* $\Delta\mathbf{k}/\mathbf{k}$, A_0 *values calculated with* $\lambda_0 = 0{\cdot}60$ Å *and smearing in* A, *expressed as* $\Delta A/\pi$

$\Delta R^y/R^y_{\text{mean}}$ represents the maximum deviation of R^y_H from the mean value $R^y_{\text{mean}} = \pi/2$, averaged over the ΔA range. For deriving $\Delta R^y/R^y_{\text{mean}}$ it was assumed that A_0 is known only within $\pm\pi/2$.

		Silicon *A*			Silicon *B*			Silicon *C*		
h k l	$\Delta\mathbf{k}/\mathbf{k}$ (%)	A_0	$\Delta A/\pi$	$\Delta R^y/R^y_{\text{mean}}$ (%)	A_0	$\Delta A/\pi$	$\Delta R^y/R^y_{\text{mean}}$ (%)	A_0	$\Delta A/\pi$	$\Delta R^y/R^y_{\text{mean}}$ (%)
0 2 2	±1·7	46·0	±0·25	±4·9	85·4	±0·5	0	123·1	±0·7	0
0 0 4	±2	45·2	±0·3	±3·9	83·8	±0·5	0	120·8	±0·8	0
0 4 4	±1	43·6	±0·15	±7·0	80·9	±0·25	±3·7	116·6	±0·35	±1·7
0 2 6	±1	42·8	±0·15	±7·0	79·5	±0·25	±3·7	114·5	±0·35	±1·7
0 0 8	±0·5	40·8	±0·05	±8·7	75·6	±0·12	±5·7	109·0	±0·17	±4·3
0 6 6	±0·5	40·1	±0·05	±8·7	74·4	±0·12	±5·7	107·2	±0·17	±4·3

temperature parameters B of Si. The observed discrepancies between α_{c-b} and α_{b-a} values at high $(\sin\theta/\lambda)^2$, which we have ascribed mainly to multiple-scattering effects, indicate that the pure kinematic treatment of TDS in perfect crystals may not be completely adequate.

By discussing the influence of the scan volume covered in reciprocal space on the amount of TDS, it became clear that the derivation of an overall ΔB can only be a rough approximation. It would be preferable to make an individual TDS correction on each measured reflection. This, however, is not feasible with the method discussed in this paper. Experimental progress can be expected to stem from the future use of the spin-echo neutron diffraction technique (Hayter, Lehmann, Mezei & Zeyen, 1979).

The authors would like to thank Professor H. Dachs for his support and advice. We are also indebted to Professor U. Bonse and Drs N. Hansen and P. Pattison for helpful discussions.

APPENDIX

Effects of dynamical diffraction and instrument resolution on the accuracy of the TDS profiles

The subtraction technique for evaluating the TDS correction factors α is based on the assumption that the elastic scattering is the same for all three crystals at a given reflection independent of their thickness. This assumption, however, is not strictly valid and the possible error introduced by neglecting the thickness dependence of the elastic scattering must be investigated in detail taking into account dynamical diffraction theory and the instrument resolution of our experiment.

The integrated reflecting power, R_{dyn}, measured in symmetric Laue geometry shows fluctuations as a function of the parameter A according to

$$R_{\text{dyn}} = R^y_H |F| \lambda^2/(\pi v_0 \sin 2\theta),$$

where

$$R^y_H = \frac{\pi}{2}\int_0^{2A} J_0(x)\,\mathrm{d}x$$

and F, λ, v_0 and θ have their usual meanings (Rauch & Petrascheck, 1978). R_{dyn} is measured on the angular scale and R^y_H is the integrated reflecting power on the dimensionless y scale. $J_0(x)$ is the zero-order Bessel function and A is given by

$$A = \lambda |F| t_0/(v_0 \cos\theta).$$

In Fig. 7, R^y_H is plotted for four ranges of A. After a nearly linear ascent, R^y_H starts to oscillate with decreasing amplitude around a mean value $\pi/2$ with a periodicity of π. The fluctuations of R^y_H are about ±11% for A around 40, ±6% for A around 80 and still ±5% for A around 120. These ranges of A correspond

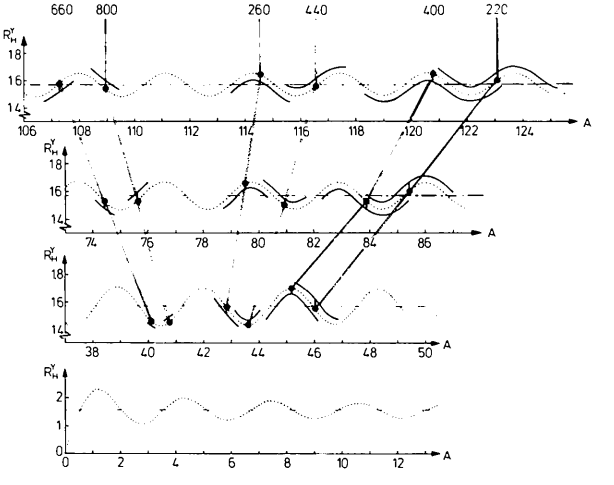

Fig. 7. The dynamic reflecting power R^y_H plotted as a function of A for four ranges of A. After a nearly linear ascent R^y_H (dotted line) starts to oscillate around the mean value $\pi/2$. The upper three A ranges around 40, 80 and 120 correspond to the experimental conditions for the crystals A, B and C, respectively. The full circles denote A_0 values calculated with $\lambda_0 = 0{\cdot}60$ Å. The wavy lines above and below the dotted line indicate the smearing in A caused by the wavelength spread. Note the different scaling of the ordinate in the lowest A range.

to the experimental conditions for the crystals A, B and C, respectively.

The limited instrument resolution, however, implies that the measurements were carried out using a wavelength band rather than a well defined wavelength. From the instrument parameters $\alpha_1 = 20'$ (collimation of the white neutron beam), $\beta_0 = 12'$ (mosaic spread of the monochromator) and $\alpha_2 > (\alpha_1^2 + 4\beta_0^2)^{1/2}$ (collimation between monochromator and sample) the wavelength spread per scan point can be estimated (see, for example, Kalus & Dorner, 1973). The resulting smearing in A is indicated by the full lines above and below the dotted line in Fig. 7 and it is listed in Table 5, expressed as $\Delta A/\pi$. For $\Delta A/\pi < \pm\frac{1}{2}$ the average value of R_H^y depends on the exact value of A_0, the mean A value. Assuming that A_0 is known only within an uncertainty of $\pm\pi/2$, we calculated the maximum deviation of R_H^y, averaged over the ΔA range, from the mean value $R^y_{\text{mean}} = \pi/2$. From these deviations, expressed as $\Delta R^y/R^y_{\text{mean}}$ in Table 5, the errors S_{osc} listed in Table 3 were derived. The S_{osc} values represent the maximum errors introduced into α by the oscillations of R_H^y.

References

ALDRED, P. J. E. & HART, M. (1973). *Proc. R. Soc. London Ser. A*, **332**, 223–254.

BÄRNIGHAUSEN, E. (1978). *J. Appl. Cryst.* **11**, 221–228.

BRUGGER, R. M. (1976). *Nucl. Instrum. Methods*, **135**, 289–291.

COOPER, M. J. (1971). *Acta Cryst.* A**27**, 148–157.

COPPENS, P. (1974). *LINEX*. Chemistry Department, State Univ. of New York at Buffalo, Buffalo, New York 14214, USA.

FREUND, A. (1980). Internal scientific report, Institut Laue–Langevin, Grenoble, France.

HAYTER, J. B., LEHMANN, M. S., MEZEI, F. & ZEYEN, C. M. E. (1979). *Acta Cryst.* A**35**, 333–336.

KALUS, J. & DORNER, B. (1973). *Acta Cryst.* A**29**, 526–528.

LARSEN, F. K., LEHMANN, M. S. & MERISALO, M. (1980). *Acta Cryst.* A**36**, 159–163.

MCSKIMIN, H. J. (1953). *J. Appl. Phys.* **24**, 988–997.

MERISALO, M. & KURITTU, J. (1978). *J. Appl. Cryst.* **11**, 179–183.

NILSSON, N. (1957). *Ark. Fys.* **12**, 247–257.

O'CONNOR, D. A. & BUTT, N. M. (1963). *Phys. Lett.* **7**, 233–235.

RAUCH, H. & PETRASCHECK, D. (1978). In *Neutron Diffraction*, edited by H. DACHS, pp. 303–351. Berlin–Heidelberg–New York: Springer.

SEEGER, R. J. & TELLER, E. (1942). *Phys. Rev.* **62**, 37–40.

SHULL, C. G. & OBERTEUFFER, J. A. (1972). *Phys. Rev. Lett.* **29**, 871–874.

WILLIS, B. T. M. (1969). *Acta Cryst.* A**25**, 277–300.

WILLIS, B. T. M. (1970). *Acta Cryst.* A**26**, 396–401.

ZACHARIASEN, W. H. (1945). *Theory of X-ray Diffraction in Crystals*. New York: John Wiley.

ZASIMOV, V. S., LOBANOV, N. N., RÜBIGER, J. & KUSMIN, R. N. (1976). *Phys. Status Solidi A*, **38**, K45–K47.

Acta Cryst. (1981). A**37**, 871–875

Investigation of Long-Range Order in Protein Crystals by X-ray Diffraction

BY A. SHAIKEVITCH AND Z. KAM

Polymer Department, The Weizmann Institute of Science, Rehovot, Israel

(*Received* 21 *January* 1981; *accepted* 5 *May* 1981)

Abstract

The rate and mechanisms of growth and the final quality of crystals are related to lattice disorders and can be studied from the analysis of X-ray diffraction patterns. Crystals of proteins and other biological macromolecules display features which are different from those of inorganic crystals. In this work the long-range order of protein crystals is probed *via* the mosaic spread, with a special camera constructed for this purpose. The very small mosaic spread measured indicates almost perfect long-range order in the crystal, suggesting the absence of dislocations. This is compatible with the weak binding energies and mechanical softness of protein crystals. If indeed such crystals do not incorporate dislocations, accumulation of strain may be a possible mechanism for the cessation of growth of protein crystals. Microscopic observations of crystal growth support this idea.

0567-7394/81/060871-05$01.00